2014 IEEE International Conference on Systems, Man, and Cybernetics
October 5-8, 2014, San Diego, CA, USA

Study of the Friction Effect on the Stability of a Three-Rigid Link Object Manipulated by Two Cooperative Robot Arms

Omar Mehrez[1], Zakarya Zyada[2], Yoshikazu Hayakawa[3], Ahmed Abo-Ismail[4], Tatsuya Suzuki[5], and Shigeyuki Hosoe[6]

[1, 2, 4] *Mechatronics and Robotics Dept., Egypt-Japan Univ. of Science and Technology (E-JUST), New Borg El-Arab, Alexandria 21934, Egypt*

[2] *Mechanical Power Engineering Dept., Tanta Univ., Tanta 31511,Egypt*

[3] *Mechanical Science and Engineering Dept., Nagoya Univ., Furo-cho, Chikusa-ku, Nagoya 464-8603, Japan*

[1, 5, 6] *RIKEN-TRI Collaboration Center for Human Interactive Robot Research, Nagoya, Aichi 463-0003, Japan*

[1](omar.mehrez@ejust.edu.eg) [2](zzyada@f-eng.tanta.edu.eg) [3](hayakawa@nuem.nagoya-u.ac.jp) [4](aboismail@ejust.edu.eg)
[5](t_suzuki@nagoya.riken.jp) [6](hosoe@nagoya.riken.jp)

***Abstract* – This work presents a study of the frictional effect on the stability of a three-rigid link object manipulated by two cooperative robot arms in a plane. It is supposed that the three-rigid link object interacts with the two robot arms at multi contact points to perform the nonprehensile manipulation of the object. The object is figured out in a way such that one of the arms is in contact with two links of the object, while the other arm is free to slide along the third link. The effect of changing frictional forces at the contact points as well as their directions on the stability of the manipulated object is to be explored by defining the system constraints. A definition of what is called the "Stability Margin" is obtained. For the same orientation of the object links, the Stability Margin is a region of equilibrium contact points between the sliding arm and the corresponding object link where the robot arm could be placed in without dropping the object. Later, an experimental system consisting of a three-rigid link object and a two planar robot arms manipulation system is equipped to verify the concept.**

Keywords: Frictional contact, nonprehensile manipulation, multi-link object manipulation, cooperative robot arms.

I. Introduction

Nowadays the demand for human interactive robots to help caregivers on site is increasing. The task of lifting patient is the heaviest one in nursing care [1]. The use of the human type arms method is the most advantageous one for such task. An example is the robot developed by RIKEN-TRI collaboration center, RIBA, which uses its whole arms in human transfer, [2]. In such application the goal is to manipulate a multi-link heavy object using whole arm manipulation. Multi-link object manipulation could be considered as a framework for the most sophisticated process of the human manipulation [3]. This work presents the study of the frictional effect on the stability of a three-rigid link object manipulated by two robot arms in a plane, see Fig. 1.

Whole arm manipulation lies under the taxonomy of nonprehensile manipulation; manipulation without grasp where simple manipulators are utilized instead of complex and dexterous ones [4], [5], and [6]. The employment of forces such as Coriolis and centrifugal forces increases the DOFs of the utilized manipulators [7], [8].

For nonprehensile manipulation, both of the object and the manipulator geometries are important. Geometry of the object is critical in determining its controllability, while that of the manipulator and its kinematics are important to establish how the manipulator can contact the object and apply appropriate forces [9], and [10].

Many applications for nonprehensile manipulation can be found in the literature, such as the quasi-static manipulation of an object by pushing [11] and sliding [12]. The dynamic manipulation like throwing and catching a disc using two planar manipulators is presented in [13]. A similar work is introduced for a polygon object using two 3-DOF manipulators in [14]. In [15], a motion planning of a planner robot to throw an object in the horizontal plane is performed. An interesting mechanism inspired from the handling of a pizza peel is implemented in [16].

However, most of the previous work is relevant to the manipulation of a 1-DOF object using one or more manipulator. Regarding the problem of manipulating a multi-link object, not so much work is found in the literature. An earlier study for manipulating a multi-link object using two cooperative robot arms is found in [3], in which the basic task requirements, conditions and difficulties are described. A more mature study have been extended to deal with the manipulation of a two-rigid link object constrained by a two cooperative robot arms [17], [18], and [19]. A dynamic model of the system has been derived, static analysis has been considered and a controller for lifting up the object in a plane has been designed. The object's behaviors were considered with and without friction contacts with the arms.

In this work, we propose a three-rigid link object manipulated by a two robot arms in a two dimensional space. Two links are always kept in contact with one arm, while the third link is in contact with the other arm, see Fig. 1. This configuration is more realistic to a lifted human rather than the one considered in [18], [19]. A previous work of the authors has been done on the dynamic modeling of such configuration in addition to the static analysis to define the equilibrium contact points [20]. This earlier study introduced the static analysis with neglecting the frictional contact, and when considering the effect of changing the friction directions at the contact points. A conclusion was: the orientation of the link-3 required for equilibrium is dependent on the directions of the friction forces. Here, a new constraint is added of keeping the orientation of link-3 fixed, and discussing the effect of changing the frictional forces as well as their directions on the system stability. The change of the friction forces is based on the idea of the friction cone, where the object will slide over the arms once the frictional forces exceed certain limits.

The paper is organized as follows: the dynamic model that represents a three-rigid link object manipulated by a two

978-1-4799-3840-7/14/$31.00 ©2014 IEEE

cooperative arms in a plane is introduced in section II. The static analysis with the consideration of the frictional forces at the contact points is performed in section III, leading to a new definition of what is called the "Stability Margin". Section IV presents discussion of the behavior of the stability margin and parameters affecting on it. Conclusions and recommendations for future work are presented in section V.

II. System Dynamics

A. System Description

Fig. 1 illustrates the schematic diagram of the system. The object is represented by three rigid links (link-1, link-2, and link-3) connected by two passive joints: the knee and the hub joints. The angular positions of the links are given by $\theta_1, \theta_2,$ and θ_3 respectively, see fig. 1. The position of the knee joint (x, y) is referred to the world coordinate frame $\sum_o$. The position of the hub joint is related to that of the knee one in terms of the length of link-2, L_2 and its angle θ_2 by the equation:

$$\begin{aligned} x_h &= x + L_2 \cos\theta_2 \\ y_h &= y + L_2 \sin\theta_2 \end{aligned} \tag{1}$$

The position of either the knee or the hub joint along with the angular positions of the three links complete the definition of the position and orientation of the object relative to $\sum_o$. The masses and mass moment of inertia of the links are denoted by m_1 and J_1, m_2 and J_2, m_3 and J_3 for link-1, link-2, and link-3 respectively. The distance from the knee joint to the center of gravities of link-1, -2 are denoted by L_1, L_{2k} respectively, and the distance from the hub joint to the center of gravity of link-3 is indicated by L_3. The object is held by two arms of radius r. The position of each arm relative to $\sum_o$ is given as (x_{Aj}, y_{Aj}), where $j = 1,2$.

Arm-1 is in contact with link-1 with interaction forces F_1 of distance l_1 and F_2 of distance l_2 from the knee joint respectively, whereas arm-2 is in contact with link-3 only with an interaction force F_3 of distance l_3 from the hub joint. The interaction force is decomposed into two components: the normal and the tangential forces F_N and F_T, respectively.

The following assumptions are considered:

1) Both of the object links and the robot arms are rigid
2) The contact between the object links and the arms is rigid.
3) The contact between the arms and the object links in a plane is a point.

B. Dynamic Modeling

The state vector which is required to completely define the object pose can be defined by:

$$q = [x \quad y \quad \theta_1 \quad \theta_2 \quad \theta_3]^T \tag{2}$$

The dynamic model of the system is obtained using the Lagrange method in the direction of the state variables, then putting in the form:

$$M(q)\ddot{q} + C(q,\dot{q})\dot{q} + G(q) = B(q,l)u \tag{3}$$

The terms $M(q), C(q,\dot{q}),$ and $G(q)$ are defined in [20]. $B(q,l)$ and u are defined by:

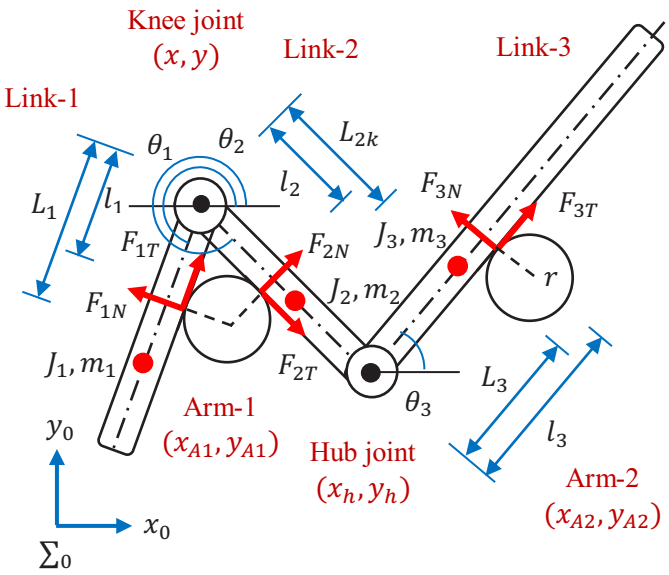

Fig. 1. System schematic diagram

$$B(q,l) = \begin{bmatrix} 1 & 0 & 1 & 0 & 1 & 0 \\ 0 & 1 & 0 & 1 & 0 & 1 \\ -l_1 \mathrm{s}\,\theta_1 & l_1 \mathrm{c}\,\theta_1 & 0 & 0 & 0 & 0 \\ 0 & 0 & -l_2 \mathrm{s}\,\theta_2 & l_2 \mathrm{c}\,\theta_2 & 0 & 0 \\ 0 & 0 & 0 & 0 & -l_3 \mathrm{s}\,\theta_3 & l_3 \mathrm{c}\,\theta_3 \end{bmatrix}, \tag{4}$$

$$u = [u_1{}^T \quad u_2{}^T \quad u_3{}^T]^T \tag{5}$$

With:

$$\begin{aligned} u_1 &= \begin{bmatrix} \sin\theta_1 & -\cos\theta_1 \\ -\cos\theta_1 & -\sin\theta_1 \end{bmatrix} \begin{bmatrix} F_{1N} \\ F_{1T} \end{bmatrix} = \begin{bmatrix} F_{1x} \\ F_{1y} \end{bmatrix} \\ u_2 &= \begin{bmatrix} -\sin\theta_2 & \cos\theta_2 \\ \cos\theta_2 & \sin\theta_2 \end{bmatrix} \begin{bmatrix} F_{2N} \\ F_{2T} \end{bmatrix} = \begin{bmatrix} F_{2x} \\ F_{2y} \end{bmatrix} \\ u_3 &= \begin{bmatrix} -\sin\theta_3 & \cos\theta_3 \\ \cos\theta_3 & \sin\theta_3 \end{bmatrix} \begin{bmatrix} F_{3N} \\ F_{3T} \end{bmatrix} = \begin{bmatrix} F_{3x} \\ F_{3y} \end{bmatrix} \end{aligned} \tag{6}$$

The distances l_1, l_2, and l_3 are given as a function of the positions of the two robot arms by:

$$\left.\begin{aligned} l_1 &= (y_{A1} - y)\sin\theta_1 + (x_{A1} - x)\cos\theta_1 \\ l_2 &= (y_{A1} - y)\sin\theta_2 + (x_{A1} - x)\cos\theta_2 \\ l_3 &= (y_{A2} - y_h)\sin\theta_3 + (x_{A2} - x_h)\cos\theta_3 \end{aligned}\right\} \tag{7}$$

The relative velocities v_1, v_2, and v_3 are given as a function of the velocities of the robot arms by:

$$\left.\begin{aligned} v_1 &= (\dot{y}_{A1} - \dot{y})\sin\theta_1 + (\dot{x}_{A1} - \dot{x})\cos\theta_1 \\ v_2 &= (\dot{y}_{A1} - \dot{y})\sin\theta_2 + (\dot{x}_{A1} - \dot{x})\cos\theta_2 \\ v_3 &= (\dot{y}_{A2} - \dot{y}_h)\sin\theta_3 + (\dot{x}_{A2} - \dot{x}_h)\cos\theta_3 \end{aligned}\right\} \tag{8}$$

C. Contact Model

The contact between the arm and the object is described by the rigid contact model where the stiffness of the arm k is considered large enough to prevent any deformation could be result in it, i.e.; its value is going to infinity. F_{iN} is calculated from the relation, where $i = 1,2,3$:

$$F_{iN} = {}^{\tau_{\theta_i}}/_{l_i} \tag{9}$$

Where, τ_{θ_i} is the torque around the knee joint for link-1 and link-2, and around the hub joint for link-3

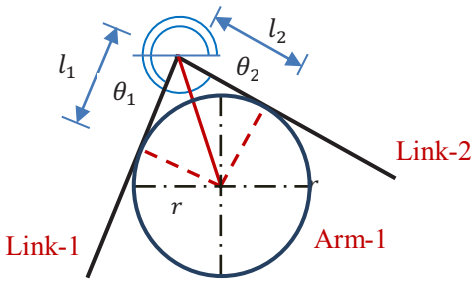

Fig. 2. Kinematic constraint of link-1 and link-2

D. Kinematic Constraint of Link-1 and Link-2

Since arm-1 is kept in contact with both link-1 and link-2, see fig. 2, the contact lengths l_1 and l_2 are obtained from the relation:

$$l_1 = l_2 = r/\tan\left(\frac{\theta_2 - \theta_1}{2}\right) \tag{10}$$

III. Frictional Static Analysis

A. Purpose of the Static Analysis

The scope of the static analysis is to obtain the equilibrium contact points between the object and the arms (i.e.; the contact lengths l_i) required to statically hold the object at different configurations. At these contact points, the two robot arms are capable of providing the interaction forces balancing with the object gravity forces.

In previous work [20], performing the static analysis with neglecting the friction forces at the contact points led to the following: for each configuration of link-1 and link-2, i.e.; θ_1 and θ_2, there is a specified orientation of link-3, θ_3, required for a stable balance of the object. As the difference between θ_1 and θ_2 increases, the corresponding θ_3 is also increasing, see fig. 3. l_i change with θ_i, i.e.; only certain $l_1, l_2,$ and $l_3,$ are required for certain $\theta_1, \theta_2,$ and θ_3. The links' angles are restricted to change within the following ranges:

$$\left.\begin{array}{c} 180° \le \theta_1 \le 270° \\ 270° \le \theta_2 \le 360° \\ 0° \le \theta_3 \le 90° \end{array}\right\} \tag{11}$$

Now with considering the friction at the contact points, the solution of the static problem is obtained by substituting in (3) by $\ddot{q}(t) = \dot{q}(t) = 0$. Therefore (3) will be in the form:

$$\begin{bmatrix} 0 \\ \sum m_i g \\ m_1 L_1 g \cos\theta_1 \\ (m_2 L_{2k} + m_3 L_3) g \cos\theta_2 \\ m_3 L_3 g \cos\theta_3 \end{bmatrix} = \begin{bmatrix} \sum F_x \\ \sum F_y \\ \tau_{\theta_1} \\ \tau_{\theta_2} \\ \tau_{\theta_3} \end{bmatrix} \tag{12}$$

Where;

$$\begin{aligned} \sum F_x &= F_{1N}\sin\theta_1 - F_{2N}\sin\theta_2 - F_{3N}\sin\theta_3 \\ &\quad -F_{1T}\cos\theta_1 + F_{2T}\cos\theta_2 + F_{3T}\cos\theta_3 \\ \sum F_y &= -F_{1N}\cos\theta_1 + F_{2N}\cos\theta_2 + F_{3N}\cos\theta_3 \\ &\quad -F_{1T}\sin\theta_1 + F_{2T}\sin\theta_2 + F_{3T}\sin\theta_3 \\ \tau_{\theta_1} &= -F_{1N} l_1, \quad \tau_{\theta_2} = F_{2N} l_2, \quad \tau_{\theta_3} = F_{3N} l_3 \end{aligned} \tag{13}$$

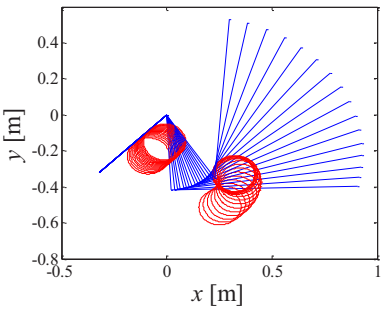

Fig. 3. Change of θ_3 with the change of the difference between θ_1 and θ_2

B. Concept of the Friction Cone

Friction is the tangential reaction force between two surfaces in contact. Static friction is the friction when sticking. The force required to overcome the static friction and initiate the motion is the breakaway force. As the interaction tangential force F_T is below the breakaway force, sticking between the two surfaces is held. Once it exceeds, relative motion between the two surfaces occurs. The static friction force F_f is related to the normal force F_N by the static friction coefficient μ_s, and its direction is varied according to the trend of the relative motion between the two surfaces:

$$F_f = [-\mu_s F_N, \mu_s F_N] \tag{14}$$

The interaction tangential force F_T is equal in magnitude and opposite in direction to F_f:

$$F_T = -F_f \tag{15}$$

The friction cone is a cone in which the tangential force F_T must be located, when both surfaces are at rest. The max cone angle α_{max} is determined by the value of μ_s, see fig. 4.

$$\alpha_{max} = \tan^{-1}\mu_s = F_T/F_N \tag{16}$$

C. Proposed Algorithm

The concept of the friction cone is utilized in solving the static problem when considering the fictional effect at the contact points. The following constraints are assumed:

1) θ_3 is deduced from the frictionless analysis for specified values of θ_1 and θ_2 [20], and this object configuration is held constant throughout the analysis.
2) F_{iT}, at the three contact points, is bounded within the limits $[-\mu_s F_{iN}, \mu_s F_{iN}]$, and if one of them exceeds its corresponding limits, sliding of the object over the arms will occur.

The procedure of the solution for a specified values of θ_1, θ_2, and θ_3 is going as follows:

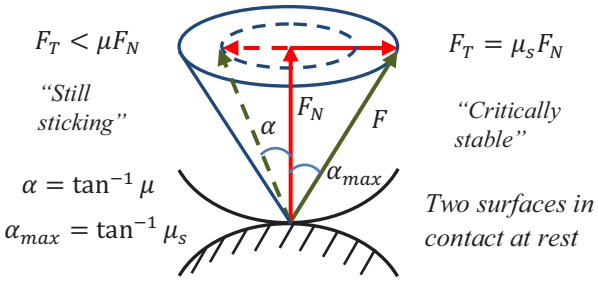

Fig. 4. Friction cone concept

1. l_1 and l_2 are determined from (10).
2. F_{1N} and F_{2N} are determined from (9).
3. F_{1T} and F_{2T} are changing according to (14) and (15).
4. F_{3N}, F_{3T} and l_3 are determined by reformulating (12) as:

$$F_{3N} = \sum m_i\, g \cos\theta_3 + F_{1N}\cos(\theta_1 - \theta_3) - F_{2N}\cos(\theta_2 - \theta_3) + F_{1T}\sin(\theta_1 - \theta_3) - F_{2T}\sin(\theta_2 - \theta_3) \quad (17)$$

$$F_{3T} = \sum m_i\, g \sin\theta_3 - F_{1N}\sin(\theta_1 - \theta_3) + F_{2N}\sin(\theta_2 - \theta_3) + F_{1T}\cos(\theta_1 - \theta_3) - F_{2T}\cos(\theta_2 - \theta_3) \quad (18)$$

$$l_3 = \tau_{\theta_3}/F_{3N} \quad (19)$$

5. Since F_{1N} and F_{2N} are constant for fixed θ_1 and θ_2, F_{3N} and F_{3T} (and hence l_3) depend only on the change of F_{1T} and F_{2T}. F_{3N}, F_{3T}, and l_3 are accepted as equilibrium values only and only if F_{3T} satisfies (14), i.e.; lies within the friction cone limits of its corresponding calculated F_{3N}. l_3 is considered, in this case, an equilibrium contact length.

F_{1T} and F_{2T} are changed by changing the angle of the friction cone, i.e.; changing μ such that its maximum value is equal to μ_s, larger than this angle sliding will occur.

The difference between the maximum and minimum values of l_3 is calculated, introducing a new definition of the; Stability Margin Δl_3. It is a region of equilibrium points where arm-2 could be put and stably hold the object for constant θ_1, θ_2, and θ_3. Fig. 5 and 6 illustrate the concept of the stability margin, and the flow chart of the proposed algorithm respectively. Values of the parameters used in the simulation are given in Table1 in the Appendix.

$$\Delta l_3 = l_{3max} - l_{3min} \quad (20)$$

IV. Discussion of the Stability Margin

A. Behavior of the Stability Margin at Different Configurations

To study the behavior of the stability margin, the proposed algorithm is repeated for different orientations such that: $\theta_1 = 250\text{deg}$, changing $\theta_2 = 270\sim360\text{deg}$ and calculating corresponding $\theta_3 \in [0{:}\,90]\text{deg}$, see fig.3.

As θ_2 increases (and hence θ_3), Δl_3 increases till it reaches its maximum at certain value of θ_2, then it decreases. At some specified values of θ_2, discontinuity in Δl_3 starts. The reasons of this discontinuity will be discussed in the next paragraph. Fig. 7 illustrates the change of Δl_3, with both θ_2 and θ_3. Fig. 8 shows the change of l_3 with θ_2. The change with θ_3 will be the same.

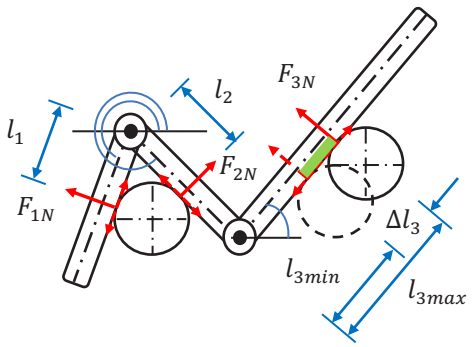

Fig. 5. Concept of the stability margin

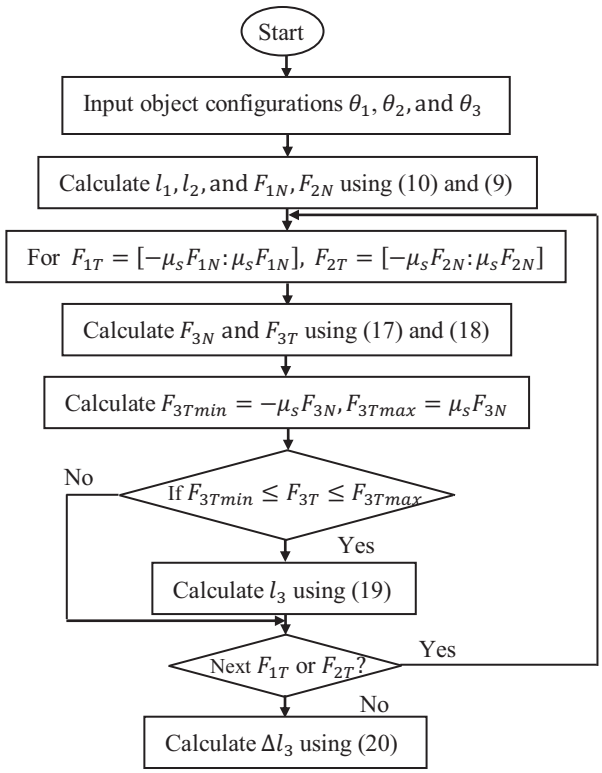

Fig. 6. Flow chart of the proposed algorithm

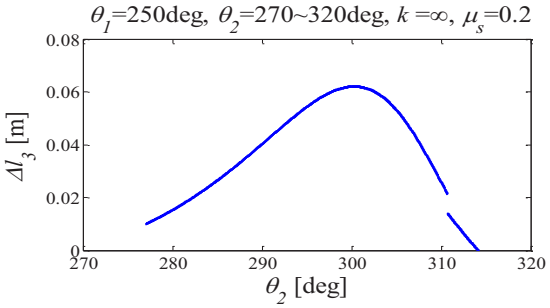

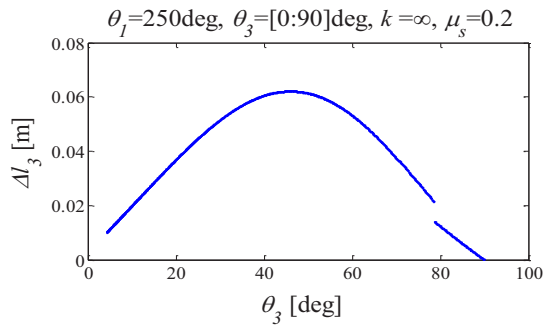

Fig. 7. Change of Δl_3 with θ_2 and θ_3

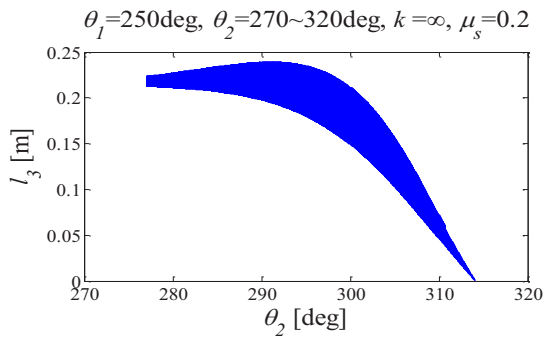

Fig. 8. Change of l_3 with θ_2

B. Discontinuity in the Stability Margin

To explore the reasons of the discontinuity, the following procedure is applied:

1) Parameters affecting l_3 are firstly discussed by taking a point located in the continuous margin, e.g. $\theta_2 = 300\text{deg}$,

2) Showing the effect of these parameters on points located in the discontinuity margin e.g. $\theta_2 > 309\text{deg}$,

Firstly, a point within the continuous margin:

For $\theta_1 = 250\text{deg}$, $\theta_2 = 300\text{deg}$, and corresponding $\theta_3 = 46\text{deg}$, F_{1N} and F_{2N} becomes constant. So the change of l_3 depends on the change of the value and direction of F_{1T} and F_{2T}. The same is as for F_{3N} and F_{3T}, see fig. 9.

F_{3T} is strongly dependent on F_{2T}, its direction is the same as of F_{2T}. F_{3N} is minimum when F_{3T} is maximum in the negative direction, and vice versa. l_3 is inversely proportional to F_{3N}. Fig. 10 shows the conditions of $l_{3\min}$ and $l_{3\max}$, and their corresponding F_{3N} and F_{3T}.

Secondly, points within the discontinuous margin:

For $\theta_2 > 309\text{deg}$, some values of l_3 are not considered as equilibrium ones, since they are not achieving the condition (13), i.e. sliding of the object over the arm will occur at these points.

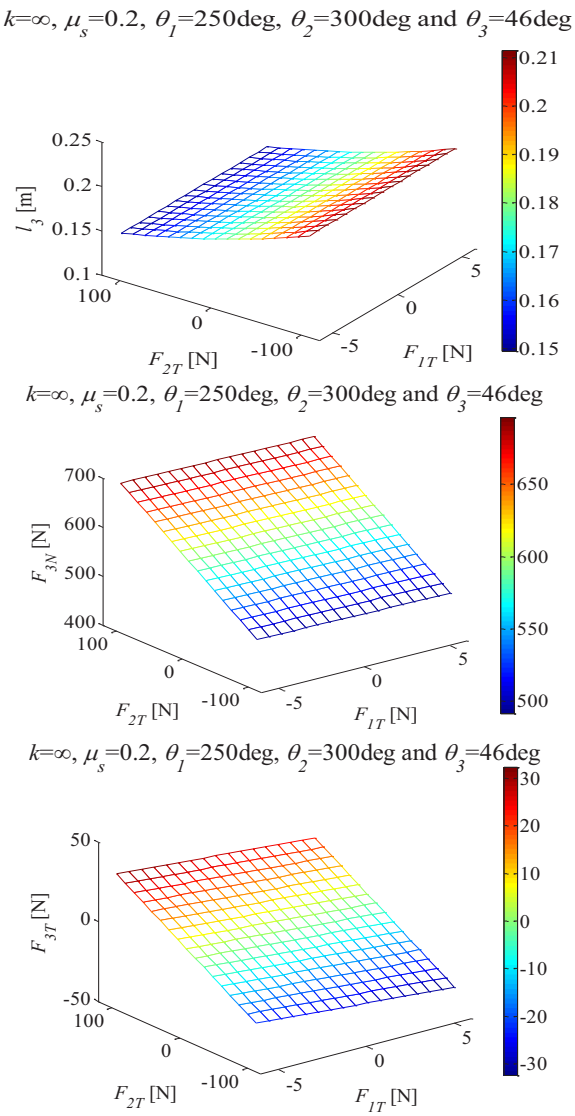

Fig. 9. Change of l_3, F_{3N}, and F_{3N} with F_{1T} and F_{2T}

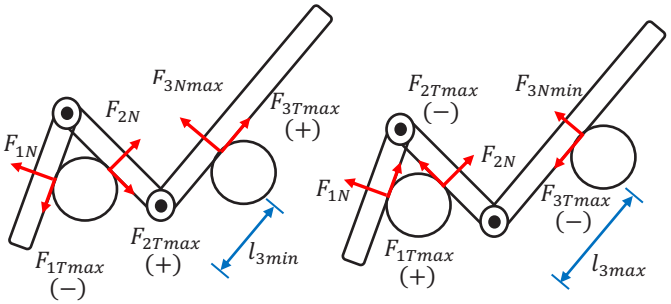

Fig. 10. Conditions of the stability margin boundaries

This happens at $F_{3\text{Nmin}}$, where F_{3T} is max. in the negative direction, refer to fig. 10. The trend of Δl_3 will change, resulting in this discontinuity, see fig. 11.

Fig. 12 enhances the concept of the reasons of the discontinuity due to not satisfying the no-sliding condition at F_{3T}. Δl_3 is plotted against θ_2 in both cases; not considering the no-sliding condition; and with considering it in the algorithm. The two curves are identical till the start of the discontinuity.

Discontinuity occurs at larger θ_2 values for the same θ_1 value, because l_1 and l_2 decrease as a result of increasing the difference between θ_1 and θ_2.

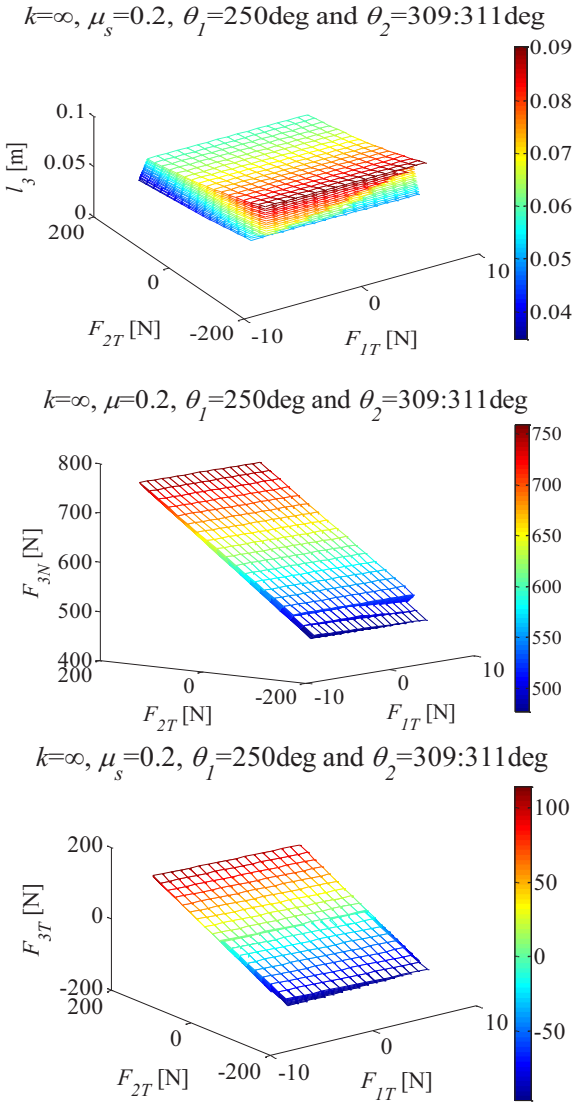

Fig. 11. Change of l_3, F_{3N}, and F_{3N} at discontinuity points

F_{1N} and F_{2N} increase and hence the range of F_{1T} and F_{2T}. F_{3T} also increases and at certain values it becomes out of the boundaries of sticking. Fig. 13 shows the change of l_3 with the increase of θ_2. Fig. 14 shows the volumetric representation of l_3 at different θ_2 values without and with the consideration of the no-sliding condition at fixed θ_1 value.

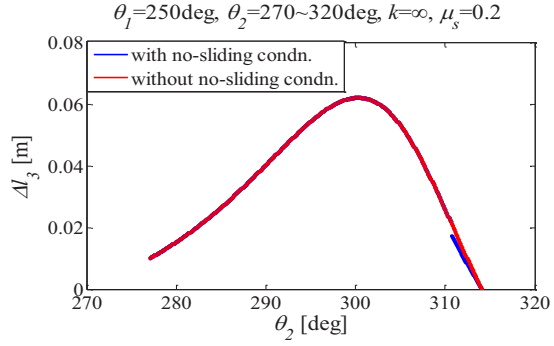

Fig. 12. Change of Δl_3 with θ_2 with/without sliding cond.

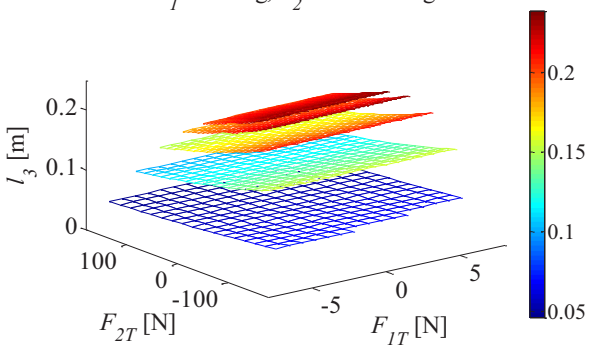

Fig. 13. Change of l_3 with increasing θ_2.

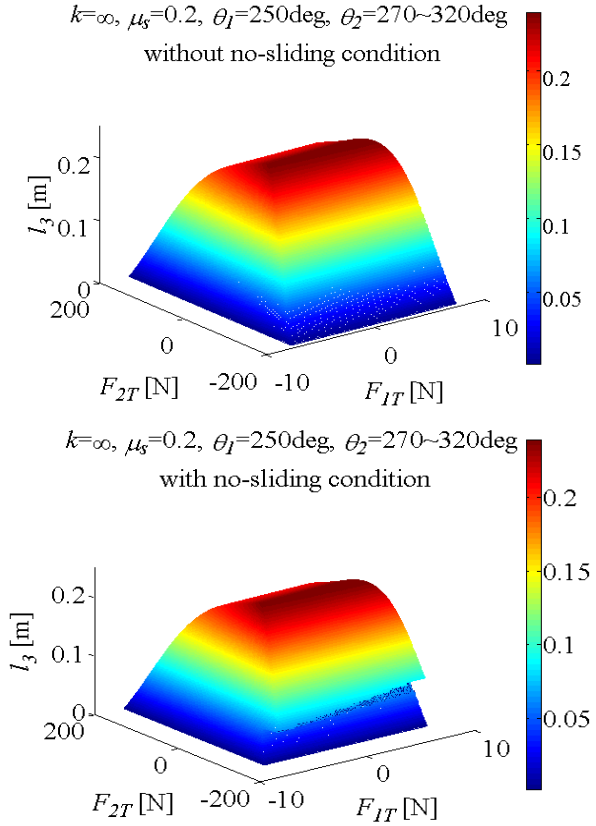

Fig. 14. Volumetric representation of l_3 without/with considering the no-sliding condition

The effect of the change of θ_1 on Δl_3 is given in fig 15. Δl_3 is plotted against θ_2 and θ_3 at different θ_1. The maximum Δl_3 is obtained when link-1 is set vertically. Fig. 16 shows the volumetric representation of Δl_3 against θ_2 and θ_3 after removing the discontinuity margins; the aggregation of the previous three figures.

C. Changing the Static Friction Coefficient

Increasing the static friction coefficient μ_s has the effect of increasing Δl_3, but at the expense of increasing the discontinuity. Δl_3 is plotted against both θ_2 and θ_3 for the same θ_1, see fig. 17.

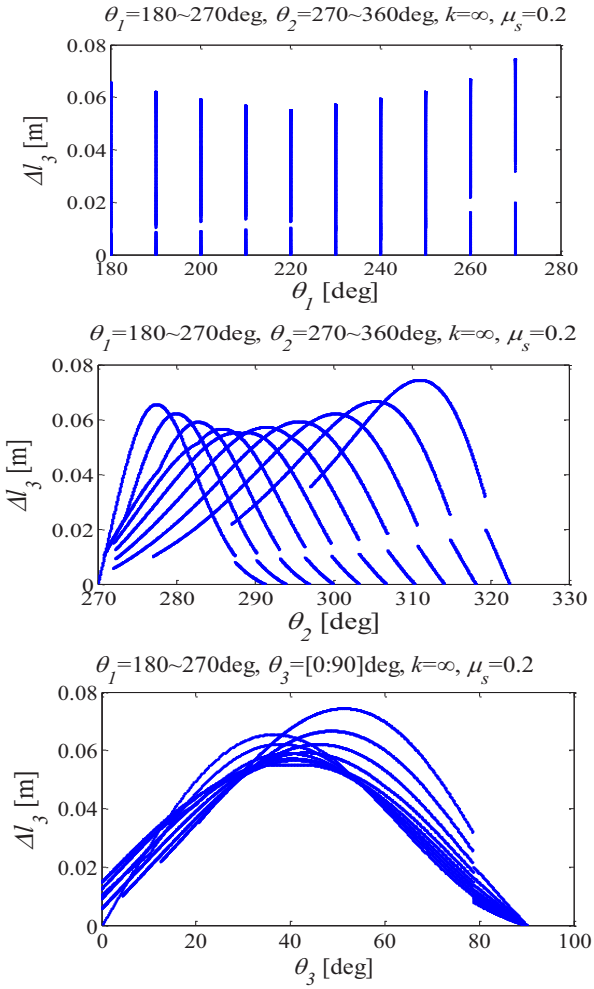

Fig. 15. Change of Δl_3 with θ_1

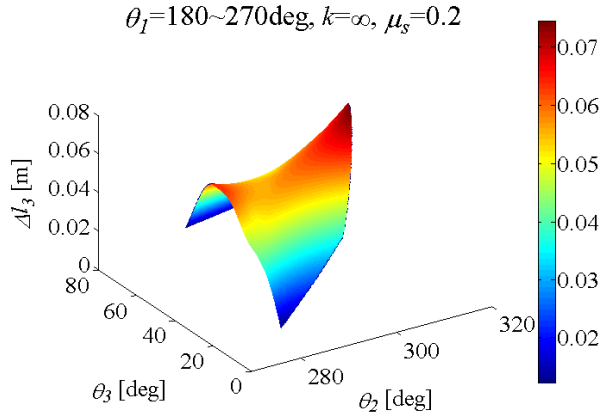

Fig. 16.Volumetric representation of Δl_3 at different configurations

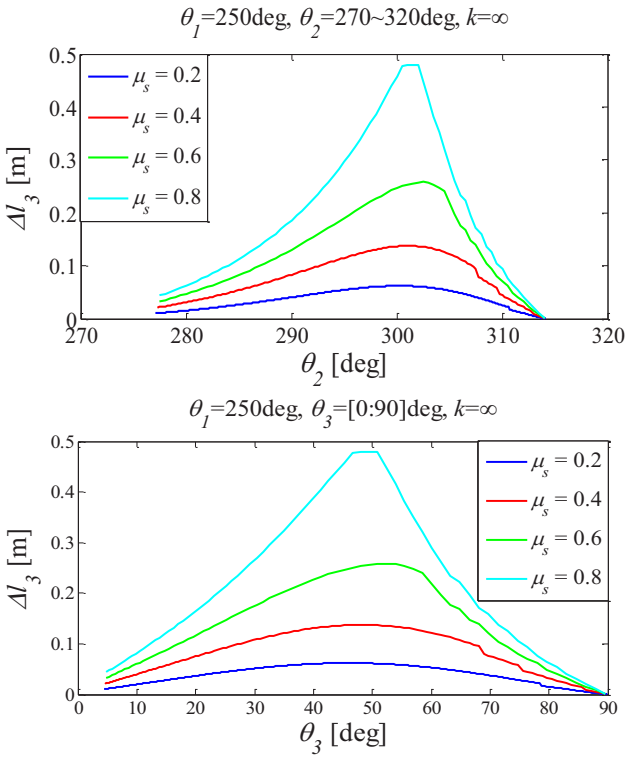

Fig. 17. Change of Δl_3 with μ_s at certain θ_1

V. CONCLUSIONS

The effect of the static friction on the stability of a three-rigid link object manipulated by two cooperative robot arms in a plane, is discussed. The two arms interact with the object at three contact points. One of the two arms is kept in contact with two links of the object, while the other arm is free to slide along the third link, and proposing rigid contact in all cases. Static analysis has been performed to obtain the position of the robot arms required to stably hold the object at certain configuration. As a result of the static friction effect, the second robot arm could be put at any point of a certain regime for the same configuration and achieve the equilibrium. This is in contrast to the frictionless case, where only one point achieves the equilibrium. This region is called as the *Stability Margin,* and it is characterized as a function of the object orientation and the static friction coefficient. Applying an experimental verification of the concept is going on as a future work.

ACKNOWLEDGEMENT

The first author is supported by a scholarship from the Mission Department, Ministry of Higher Education of the Government of Egypt which is gratefully acknowledged.

REFERENCES

[1] Mukai, T.; Hirano, S.; Nakashima, H.; Kato, Y.; Sakaida, Y.; Guo, S.; Hosoe, S., "Development of a nursing-care assistant robot RIBA that can lift a human in its arms," *IEEE/RSJ International Conference on Intelligent Robots and Systems (IROS), 2010*, pp.5996,6001, 18-22 Oct. 2010.

[2] Mukai, T.; Hirano, S.; Yoshida, M.; Nakashima, H.; Guo, S.; Hayakawa, Y., "Whole-body contact manipulation using tactile information for the nursing-care assistant robot RIBA," *IEEE/RSJ International Conference on Intelligent Robots and Systems (IROS), 2011*, pp.2445, 2451, 25-30 Sept. 2011.

[3] Onishi, M.; Odashima, T.; Zhiwei Luo, "Emergent cooperative manipulation of a multi-linked object," *Annual Conference SICE 2003*, vol.3, pp.3049, 3052, 4-6 Aug. 2003.

[4] Maeda, Y.; Nakamura, T.; Arai, T.; "Motion Planning of Robot Fingertips for Graspless Manipulation", *IEEE International Conference on Robotics & Automation, 2004*, pp.2951, 2956, 24 April-1 May 2004.

[5] Lynch, K.M.; Shiroma, M.; Arai, T.; Taniez, K.; "The roles of shape and motion in dynamic manipulation: The Butterfly Example", *IEEE International Conference on Robotics and Automation (ICRA), 1998,* pp.1958, 1963, 16 -20 May 1998.

[6] Mason, Matthew T.; Lynch, K.M., "Dynamic manipulation," *IEEE/RSJ International Conference on Intelligent Robots and Systems (IROS) 1993*, pp.152, 159, 26-30 Jul 1993.

[7] Asano, F.; Saitoh, Y.; Watanabe, K.; Zhi-Wei Luo; Yamakita, M.; "On dynamic whole body manipulation," *IEEE International Symposium on Computational Intelligence in Robotics and Automation, 2003*, vol.3, pp.1201, 1206, 16-20 July 2003.

[8] Lynch, K.; and Mason, M.; "Dynamic nonprehensile manipulation: controllability, planning, and experiments," *International Journal of Robotics Research,* vol.18, no.1, pp. 64, 92, 1999.

[9] Lynch, K. M. and Black, C. K.; "Control of underactuated manipulation by real-time nonlinear optimization", *Int. Symposium Robotics Research*, *Snowbird UT, 1999.*

[10] Lynch K. M., Murfey T. D., "Control of nonprehensile manipulation," CPRA, 2002.

[11] Lynch K. M.; "Locally controllable polygons by stable pushing," *IEEE International Conference on Robotics and Automation (ICRA), 1997*, pp.1442-1447, 20-25 Apr. 1997.

[12] Goyal, S.; Ruina, A.; Papadopoulos, J.; "Planar sliding with dry friction. Parts 1, 2: Limit surface and moment function. Wear" 143:307–330. 1991

[13] Beigzadeh, B.; Ahmadabadi, M.N.; Meghdari, A.; "Two dimensional dynamic manipulation of a disc using two manipulators," *IEEE International Conference on Mechatronics and Automation (ICMA), 2006*, pp.1191, 1196, 25-28 June 2006.

[14] Akbarimajd, A. ; Ahmadabadi, M.N; "Manipulation by juggling of planar polygonal objects using two 3-DOF manipulators," *IEEE/ASME International Conference on Advanced Intelligent Mechatronics (AIM), 2007*, pp.1, 6, 4-7 Sept. 2007.

[15] Mori, W.; Ueda, J.; Ogasawara, T., "1-DOF dynamic pitching robot that independently controls velocity, Angular velocity, and direction of a ball: Contact models and motion planning," *IEEE International Conference on Robotics and Automation (ICRA), 2009*, pp.1655, 1661, 12-17 May 2009.

[16] Higashimori, M.; Utsumi, K.; Omoto, Yasutaka; Kaneko, M., "Dynamic manipulation inspired by the handling of a pizza peel," *IEEE Transactions on Robotics,* vol.25, no.4, pp.829, 838, Aug. 2009.

[17] Zyada, Z.; Hayakawa, Y.; and Hosoe, S.; "Kinematic analysis of a two-link object for whole arm manipulation," *International Conference on Signal Processing, Robotics and Automation (ISPRA), 2010,* University of Cambridge, UK, 20-22 Feb. 2009.

[18] Zyada, Z.; Hayakawa, Y.; Hosoe, S.; "Model-based control for nonprehensile manipulation of a two-rigid-link object by two cooperative arms," *IEEE International Conference on Robotics and Biomimetic (ROBIO), 2010*, pp.472, 477, 14-18 Dec. 2010.

[19] Zyada, Z.; Hayakawa, Y.; and Hosoe, S., "Fuzzy nonprehensile manipulation control of a two-rigid-link object by two cooperative arms," *18th World Congress of the International Federation of Automatic Control (IFAC), 2011.*

[20] Mehrez, O.; Zyada, Z.; Abbas, H.; and Abo-Ismail A.; "Modeling and Static Analysis of a Three-Rigid-Link Object for Nonprehensile Manipulation Planning" *IEEE International Conference on Mechatronics and Automation (ICMA), 2013*, pp.1441-1446, 4-7 Aug. 2013.

APPENDIX

TABLE 1
PHYSICAL PAAMETERS OF THE SYSTEM

Symbol		$i=1$	$i=2$	$i=3$
m_i	[Kg]	7	20	43
L_i	[m]	0.25	0.24	0.35
L_{iT}	[m]	0.45	0.42	0.88
r_i	[m]	0.1	0.1	-
J_i	[kg/m^2]	1	1	1
k_i	[N/m]	∞	∞	∞
μ_s		0.2	0.2	0.2